Materials Today Sustainability 34 (2026) 101332

Contents lists available at ScienceDirect

Materials Today Sustainability

journal homepage: www.journals.elsevier.com/materials-today-sustainability

Unlocking the cooling power of photoluminescent materials: Experimental validation of a correction procedure for effective solar reflectance measurement

Francesco Marchini [a,b], Chiara Chiatti [b,c], Claudia Fabiani [b,d], Michele Zinzi [e], Anna Laura Pisello [b,d,*]

[a] Department of Chemistry, Biology and Biotechnology, University of Perugia, Via Elce di sotto 8, Perugia, 06123, Italy
[b] EAPLAB@CIRIAF - Interuniversity Research Center, University of Perugia, Via G. Duranti 67, Perugia, 06125, Italy
[c] Department of International Human and Social Sciences, Perugia Foreigners' University, Piazza Fortebraccio 4, Perugia, 06122, Italy
[d] Department of Engineering, University of Perugia, Via G. Duranti, 93, Perugia, 06125, Italy
[e] Smart Energy Division, Energy Technologies Department, ENEA - Italian National, Agency for New Technologies, Energy and Sustainable Economic Development, Via Anguillarese 301, Rome, 00123, Italy

ARTICLE INFO

Keywords:
Photoluminescence
UHI mitigation
Passive cooling
Cool material
Energy saving
Solar reflectance

ABSTRACT

Photoluminescent (PL) materials have recently emerged as promising heat-rejecting solutions for mitigating Urban Heat Islands (UHIs), although quantifying their contribution to heat dissipation remains challenging. This study experimentally validates an innovative procedure based on optical and photometric measurements to determine the effective solar reflectance (ESR) of PL materials. By isolating the re-emission component from the overall solar response, the cooling potential of five tiles with increasing concentrations of yellow-emitting pigments is quantitatively assessed for the first time in terms of reduced solar absorption and enhanced thermal performance. The accuracy of the analytical correction in reproducing experimental reflectance data is confirmed through statistical validation (RMSE $\leq$ 3% and $R^2 \geq 0.96$). Results reveal that higher pigment concentrations improve persistent PL performance, enhancing both luminous intensity and afterglow duration, but can also induce increased surface roughness. These morphological changes promote self-absorption phenomena and quench the emission under direct solar irradiation, ultimately reducing the net PL contribution to cooling. By enabling the experimental quantification of reflected and re-emitted components of solar energy, this validated procedure provides a critical tool for assessing the performance of a broad range of PL materials in mitigating the UHI effect.

1. Introduction

Cities are becoming the epicenters of global population growth and economic activity, now home to more than half of the world's population. As a result, urban areas are responsible for roughly two-thirds of global energy consumption and more than 70% of annual carbon emissions [1]. Due to the accelerating urbanization, these factors are projected to rise further in the coming decades, highlighting the urgent need for sustainable urban planning and climate-conscious policies [2].

In fact, the replacement of natural lands due to rapid urban expansion fundamentally change physical properties of the land surface, inducing multiple environmental consequences [3]. In particular, the slow heat release characterizing engineered urban materials, such as concrete and asphalt, and the reduced evapotranspiration due to the lack of vegetation, can upset the surface energy balance [4]. Additionally, the intensification of anthropogenic activities release significant amounts of waste heat into the urban atmosphere, further compounding the warming effect [5]. All these factors drive to acknowledged phenomenon of Urban Heat Island (UHI), where urban areas are consistently warmer than their rural and suburban surroundings [6]. But the consequences of UHI extend beyond thermal discomfort, leading to higher electricity consumption and raising public health risks [7,8]. In the past few decades, huge efforts have been focused into developing new strategies to mitigate UHI effect and its associated adverse impacts [9].

In this panorama, the so-called "cool materials", i.e., materials with an enhanced capability to reflect the incident solar radiation and release the absorbed heat, has proven to be a suitable option to counterbalance urban overheating [10,11]. Several works have demonstrated

* Correspondence to: CIRIAF - Interuniversity Research Center, University of Perugia, Via G. Duranti 67, Perugia, 06125, Italy.
E-mail address: anna.pisello@unipg.it (A.L. Pisello).

https://doi.org/10.1016/j.mtsust.2026.101332
Received 4 November 2025; Received in revised form 14 January 2026; Accepted 15 February 2026
Available online 19 February 2026

Nomenclature

Acronyms

CA	Cellulose Acetate
ESA	Effective Solar Absorptance
ESR	Effective Solar Reflectance
$FTIR$	Fourier Transform InfraRed
$InGaAs$	Indium Gallium Arsenide
MAE	Mean Absolute Error
MCT	Mercury Cadmium Telluride
NC	NanoCrystal
NIR	Near InfraRed
$NMOS$	N-type Metal Oxide Semiconductor
PCM	Phase Change Material
$PDMS$	PolyDiMethylSiloxane
PL	Photoluminescence
$PMMA$	Poly(Methyl MethAcrylate)
PSA	PolyStyrene-Acrylate
$PVDF-HFP$	Poly(VinyliDene Fluoride-co-HexaFluoroPropylene)
QD	Quantum Dot
RC	Radiative Cooling
RH	Relative Humidity
$RMSE$	Root Mean Square Error
UHI	Urban Heat Island
UV	UltraViolet

Greek symbols

α	Absorptance [–]
α^*	Effective absorptance [–]
$\Delta\rho$	Difference between reflectance values [%]
ϵ	Thermal Emissivity [–]
λ	Wavelength [nm]
Φ	Solar irradiation absorbed by the sample [W/m^2]
ρ	Reflectance [–]
ρ^*	Effective Reflectance [–]
τ	Transmittance [–]

Roman symbols

L_e	Spectral radiance [W/(sr nm m^2)]
L_v	Luminance [cd/m^2]
T_{air}	Air Temperature [°C]
T_{sup}	Superficial Temperature [°C]

Subscripts

$char$	Charging photoluminescent state of the sample
$correct$	Result from analytical correction
$disc$	Discharging photoluminescent state of the sample
$inact$	Inactive state of the sample (no photoluminescence)
max	Maximum

substantial cooling effects due to the integration of cool artificial white or even colored coatings, decreasing both surface and air temperature in the built environment [12,13]. In particular, materials exploiting radiative cooling can achieve surface temperatures below ambient air even under direct solar irradiation by efficiently emitting thermal radiation towards the outer space [14]. As a drawback, the lack of tunable responses might result in non negligible penalties during the cold months of the year, depending on the microclimate characteristics of the implementation area [15,16]. Therefore, cool materials able to adjust their thermo-optical properties based on surrounding conditions, such as thermochromic and phase change materials (PCMs), have gained significant attention within the scientific community [17]. Among these, photoluminescent materials are emerging as innovative and adaptive cool materials, distinguished by their unique wavelength-conversion mechanism that enables the re-emission of absorbed sunlight at longer wavelengths, thereby reducing solar heat gain while enhancing cooling performance [18,19]. Furthermore, these technologies can be combined in composite strategies to achieve enhanced cooling performance, greater tunability, and better integration in urban settings [20,21]. Collectively, these advanced cooling strategies aim to reduce energy consumption and emissions, while also creating healthier, more resilient urban environments in the face of a warming climate.

1.1. Photoluminescence for passive cooling applications

The phenomenon of spontaneous light emission caused by the absorption of optical radiation is defined as photoluminescence (PL). According to the duration of the re-emission, PL can be divided as fluorescence, in which the radiation emission stops immediately once the excitation source is removed (within 10 ns), and phosphorescence, involving persistent radiative decay lasting even hours. For both phenomena, the emitted radiation is generally of a longer wavelength than the incident excitation, with a spectral difference between their peaks known as Stokes shift. Historically, PL has been widely used to characterize many chemical, physical and biological processes, but only in recent years has garnered attention as a possible solution to counteract UHI effects [22]. By emitting photons rather than phonons, PL materials could reduce the amount of heat stored in the bulk material in the form of sensible heat and later re-emitted as thermal radiation.

In 2016, Berdahl et al. [23] introduced for the first time the phenomenon of fluorescence as cooling strategy of objects exposed to sunlight. In particular, this study demonstrated how ruby crystals with emission in red/NIR wavelengths could remain up to 6.5°C cooler in the sun compared to a conventional non-fluorescent reference. Indeed, absorbed photons not only produce heat but also cause fluorescence, which can be seen as an additional heat rejection mechanism compared to cool materials which rely on reflection only. From this initial breakthrough, research in the field began to expand rapidly, becoming a trustworthy option among non-white heat-rejecting solution for UHI mitigation. While white heat rejecting materials face challenges in the urban scale up due to visual and radiative glare limitations, PL materials allow for the necessary color display while maintaining high net cooling power [24]. For example, Wang et al. [21] demonstrated that PL-based radiative coolers can achieve sub-ambient cooling (2–5°C) under direct sunlight. While the quantum dots (QDs) top layer converts the UV–Visible sunlight into emitted light to minimize the solar-heat gain, the underlayer strongly reflects sunlight and radiates thermal load. As demonstrated by Min et al. [25], the optimal design of wavelength conversion via the PL mechanism enables the creation of passive coolers in any desired color while still achieving sub-ambient cooling under direct solar radiation. This superior ability allows their integration into multiple urban surfaces, such as pavements [26], roofs [27], and building envelopes [28].

Additionally, PL materials do not just present a good potential for the effective rejection of the incident solar radiation, but can also provide a cost-effective lighting solution through phosphorescence mechanism [29,30].

Table 1
Comparison of different methods to measure ESR and PL cooling effect.

Ref.	Year	Method	Instrumentation	Measure	Strengths	Limitations
[34]	2023	Calorimetric	Thermocouple	Superficial temperature, PL cooling potential	Direct quantification of cooling in real-word scenario	Outdoor measurement, sensitivity to environmental factors, difficulty in reproducing non-PL reference
[23]	2016	Calorimetric	Thermistor	Superficial temperature, PL cooling potential	Use of non-fluorescent white and light gray samples of known SR as reference	Outdoor measurement, sensitivity to environmental factors
[35]	2024	Calorimetric	Thermocouple	Superficial temperature, PL cooling potential	White base and white bilayer coatings as reference	Outdoor measurement, sensitivity to environmental factors
[36]	2024	Radiometric	Radiometer with integrating sphere	PL power efficiency, PLQY, spectral characteristics	Simple and portable setup	Necessity of a specific setup, outdoor measurement
[37]	2022	Radiometric	Spectrophotometer, spectroradiometer	ESR, PL radiative flux	Use of common instrumentation, easy and fast correction algorithm	Empirical method, still not validated
[19]	2020	Radiometric	Spectrophotometer, Spectrofluorimeter, Emissometer/FTIR, Analytical balance, Calorimeter	Cooling potential, superficial temperature	Validated model applicable to all PL materials	Necessity of physical, thermal, optical, and fluorescent properties

1.2. Measuring PL cooling effect

While metrology encompasses a wide range of different techniques for the accurate characterization of PL properties [31,32], it is still complex to distinguish surface temperature reduction caused by reflection from that of PL effect, and thus to precise estimate the PL effect contribution to heat dissipation. While, for a common material, solar reflectance quantifies the fraction of incident sunlight (300–2500 nm) reflected by the surface, PL materials reject solar radiation by both reflection (light leaves at the wavelength of incidence) and photoluminescence (light leaves at a longer wavelength). This light re-emission represents an additional radiative process that can significantly reduce the effective solar heat gain and thus must be considered together with the initial reflectance.

To account for both direct reflection and PL emission, a dedicated parameter known as Effective Solar Reflectance (ESR) has been introduced by Levinson et al. [33]. As shown in Table 1, the techniques for measuring ESR, and therefore the cooling potential offered by PL, can be broadly categorized into two groups: (i) calorimetric, which define ESR from temperature changes, and (ii) radiometric, which directly detect radiation.

In calorimetric methods, the PL cooling effect is typically assessed by empirically comparing the surface temperatures of a fluorescent material and a non-fluorescent reference with matching optical properties [34]. However, fabricating such reference samples is complex and time-consuming, requiring precise control over optical characteristics to isolate the PL contribution [38]. An alternative approach leverages the linear relationship between solar absorption and surface temperature. In this case, the fluorescent sample is compared to two non-fluorescent references, one with higher and one with lower solar absorption, to estimate the cooling contribution [23]. These methods require outdoor measurements and are sensitive to environmental factors such as convective heat transfer and solar irradiance fluctuations, demanding carefully designed experimental setups [33].

Radiometric measurement of ESR, typically performed using instruments designed for solar reflectance, presents its own challenges. For example, standard solar spectrophotometers with an integrating sphere are not feasible to collect the reflectance of PL-active materials. These instruments assume that the detected light has the same wavelength as the incident (monochromatic) light. However, PL materials emit light at longer wavelengths than those used for excitation. Consequently, the detector is stimulated by emission wavelengths rather than the incident ones, leading to inaccurate reflectance measurements due to wavelength-dependent variations in detector sensitivity and instrument response. To overcome this limitation, Chiatti et al. [37] introduced a novel analytical procedure to detect the effective reflectance of a material, combining for the first time optical and photometric properties. While the method yielded promising results, it has not yet undergone experimental validation as a replicable ready-for-standard measurement protocol.

Overall, accurately determining the ESR of PL materials through experimental methods remains a key challenge that must be addressed to fully harness their potential in mitigating UHI effects [39].

1.3. Aim of the work

While highly reflective cool materials have been extensively studied for passive thermal regulation, the use of photoluminescence as heat rejection mechanism remains still under development. These materials contribute to surface cooling by absorbing part of the incident solar radiation and re-emitting it at longer wavelengths, thereby shifting a portion of the absorbed energy away from heat-generating processes. However, the development of techniques capable of quantifying the effective solar reflectance (ESR), and thereby the PL contribution to a surface's energy budget, remains an ongoing challenge.

Without a proper evaluation of ESR, the true added value of PL materials over conventional cool materials cannot be reliably assessed, limiting market investment and broader adoption. A preliminary approach to account for PL contributions to ESR was recently proposed by Chiatti et al. [37], introducing a wavelength-resolved correction factor derived from optical and photometric measurements. However, this methodology has not yet been experimentally validated against direct ESR measurements performed under controlled PL excitation.

The present work addresses this gap by providing the first experimental validation of the analytical ESR-correction method through comparison with measurements obtained using a dedicated measurement setup designed with polychromatic excitation. Unlike conventional spectrophotometers, which are inherently biased in the presence of PL, this setup enables accurate and reliable ESR detection in PL-active materials. By isolating the re-emission contribution, the validated method enables an accurate quantification of the cooling potential of PL materials in terms of reduced solar absorption and improved thermal performance. This approach, applicable to a wide range of PL materials, provides a necessary tool for evaluating their potential and enables rigorous comparison with conventional cool materials for UHI mitigation.

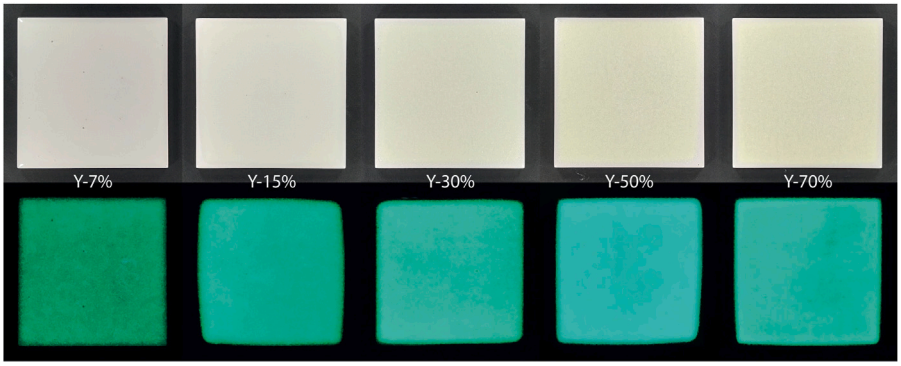

Fig. 1. Samples in their discharged (above) and charged (below) condition. (For interpretation of the references to color in this figure legend, the reader is referred to the web version of this article.)

2. Materials and methods

This section provides a structured framework to evaluate the accuracy and applicability of the proposed approach for ESR quantification of PL materials. Section 2.1 introduces the materials selected for investigation and validation. Then, a comprehensive overview of the experimental methodology and the characterization techniques adopted to assess the morphological, optical, and thermal properties of the samples is provided (Section 2.2). Subsequently, the analytical model developed to interpret the behavior of the PL materials is illustrated in detail (Section 2.3), and its experimental validation is discussed in Section 2.3.3.

2.1. Materials and samples

Since its discovery by Matsuzawa et al. in 1996 [40], europium-doped strontium aluminate ($SrAl_2O_4$: Eu^{2+},Dy^{3+}) has become the most widely used long-lasting phosphorescent material due to its high brightness, extended afterglow duration, non-toxicity, and excellent chemical stability. These pigments, showing absorption in the UV-blue wavelengths and yellow-green emission centered around 520 nm, can be dispersed into solutions to produce adaptive components capable of glowing in the dark (e.g. glasses, ceramics, polymers), making them ideal for a wide range of applications [41]. In this study, five prototypes of PL tiles (10 × 10 × 0.5(h) cm) provided by Bright Materials srl [42] were taken into account. Samples were prepared by dispersing different weight fractions (7%, 15%, 30%, 50% and 70%) of $SrAl_2O_4$: Eu^{2+},Dy^{3+} pigments in a transparent matrix and depositing the resultant PL coating as a top layer onto ceramic tiles previously covered with a white opaque glaze. The pigment concentrations were selected to cover a broad range from low to high loading, allowing the investigation of their effect on PL efficiency and thermo-optical response.

Fig. 1 shows the investigated tiles emitting a green afterglow if exposed by UV or VIS radiation. Increasing amounts of pigments result in more yellowish surfaces with greater superficial roughness.

2.2. Experimental characterization

As part of the preliminary material characterization, a roughness analysis was conducted to quantify pigment-induced surface texture variations, which may influence the optical and thermal properties of the investigated samples. The surface morphology of the samples was analyzed using a Nanovea JR25 optical profilometer, following the ISO 25178 standard [43]. Specifically, surface parameters were calculated over a 1 × 1 cm area for each sample, including height-related (Sq, Sku, Sz), spatial (Sal, Str, Std), and hybrid parameters (Sdq, Sdr).

For the optical characterization, samples were tested under three distinct conditions: (i) inactive (no afterglow emission), (ii) charging (PL under direct irradiation), and (iii) discharging (persistent PL after 1 h of exposure), as shown in Fig. 2.

The characterization of both inactive and discharging samples followed the procedures outlined by Chiatti et al. [37]. Reflectance (ρ) measurements were performed using a UV/VIS/NIR High-Performance Lambda 1050+ Spectrophotometer with a dual monochromator configuration (Fig. 3a). Sample were tested before and after exposure to a BF SUN 1200 W solar lamp, installed in an ATT DM340SR climatic chamber, under an irradiation of 1000 W/m^2 with constant temperature (T_{air} = 25°C) and relative humidity (RH = 40%) (Fig. 3b). Spectra were acquired by scanning from 2500 nm down to 250 nm (spectral resolution 1 nm) to avoid unintended photoexcitation of the PL pigment, ensuring that inactive samples remain uncharged and that charged samples were not influenced by additional excitation during the measurement itself. According to the ASTM E903 standard [44], the reflection coefficients were obtained as the mean value of three independent measurements. For charged samples, reflectance measurements were repeated every 5 min over a 2-hour period to monitor the PL afterglow decay. To avoid external light interference, the sample remained inside the spectrophotometer during the entire test.

As previously discussed, conventional spectrophotometers are inherently subject to bias, as PL emission is detected as reflected light at the monochromatic wavelength of the illumination source. To overcome this limitation, spectral reflectance measurements of the charging samples were performed using a dedicated experimental setup [45], in which white light is introduced into the integrating sphere, while wavelength selection is performed downstream, in the detection system. The instrument features a large-diameter (75 cm) integrating sphere coated internally with white Spectralon (Fig. 3c). Polychromatic excitation was provided by a 300-W xenon arc lamp (350–1600 nm) and a power-tunable 1000-W tungsten–halogen lamp (450–2300 nm). The detection system consists of a diode-array spectrophotometer, equipped with multiple sensors: (i) NMOS for the 250–1000 nm range, and (ii) InGaAs for the 900–1700 nm range. The built-in spectrophotometer is of the single-beam type, thus the raw measurements are corrected with the auxiliary port method. The measurement procedure is extensively reported in [45]. Reflectance relative measurements are performed against a calibrated withe Spectralon target with a spectral resolution of 1 nm. The overall system exhibits a measurement uncertainty of ±0.02 for relative spectral values ranging from 0 to 1. Owing to the large diameter (20 cm) of the sample port, four tiles with the same amount of PL pigments were combined to fully cover the measurement area.

A JETI Specbos 1211UV spectroradiometer was employed to accurately measure both the spectral radiance (L_e) and luminance (L_v) of the PL emission between 350–1000 nm, in accordance with DIN 67510-1 [46]. Although the radiometric data alone is not sufficient to determine the ESR, it provides essential insight into the spectral and temporal features of the PL emission, which are crucial for implementing the correction algorithm. Prior to testing, each tile was

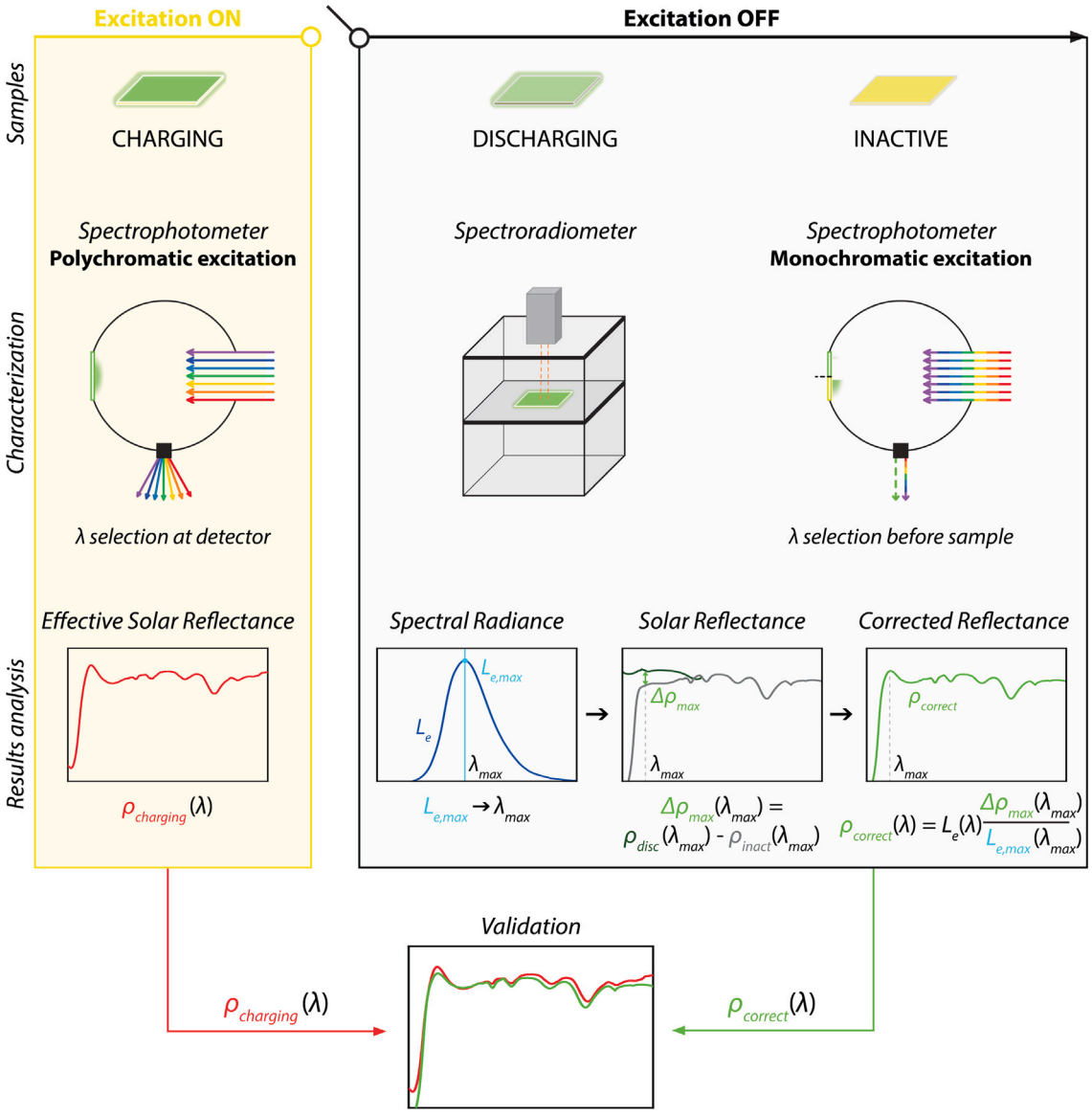

Fig. 2. Workflow of the experimental methodology used to validate the correction procedure for ESR calculation.

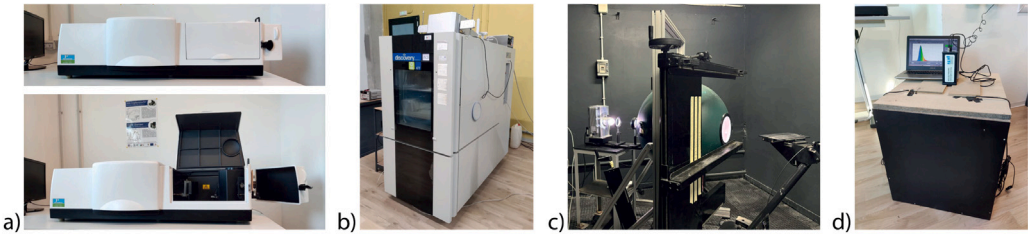

Fig. 3. Instrumentation employed for sample characterization: (a) PerkinElmer Lambda 1050+ spectrophotometer; (b) ATT DM340SR climatic chamber; (c) CATRAM setup; (d) JETI Specbos 1211UV spectroradiometer.

charged in the climatic chamber following the same conditions and timing previously described. Spectroradiometric measurements were then carried out starting immediately after the end of excitation and repeated at 5-minute intervals, continuing up to 120 min. For each sample, the experiment was repeated three times independently, and the average values and standard deviations were computed from the resulting datasets. This part of the experimental campaign required a custom setup: a matte black-coated wooden box (54 × 60 × 60 cm^3) with a removable lid, featuring a central 2.5 cm diameter hole (Fig. 3d). This hole housed the spectroradiometer detector, aimed at the tile placed inside on a shelf [47]. Based on the obtained luminance decay profiles, the PL decay time of each glass tile was calculated following DIN 67510-1, using 0.03 cd/m^2 as the threshold value to ensure comparability with reference procedure.

The thermal emissivity of the samples was characterized using two complementary methods. Hemispherical reflectance in the MIR range (2.5–20 μm) was estimated using a PerkinElmer Spectrum 3 FTIR spectrometer equipped with a gold-coated integrating sphere.

Absorbance spectra were acquired by averaging 1024 scans at a 4 cm^{-1} resolution, using a diffuse gold standard as the background reference. In addition, hemispherical thermal emissivity was directly measured using a portable differential thermopile emissometer (AE1 RD1, D&S Instruments) in accordance with ASTM C1371 [48]. The Solar Reflectance Index (SRI) of the investigated samples was calculated according to ASTM E1980-19 [49], using solar reflectance values determined according to ISO 9050 [50]. The average convective heat transfer coefficient (h_c = 12 W/m^2 K) was adopted to represent typical outdoor conditions.

2.3. Analytic interpretation

This section presents the analytical framework developed to interpret the optical behavior of PL materials and quantify their cooling performance. First, the correction algorithm for the estimation of ESR is described (Section 2.3.1). Therefore, Section 2.3.2 describes the validation of this approach through comparison with experimental data obtained from a dedicated measurement setup. Finally, the impact of the corrected ESR values on the material's cooling potential is evaluated to assess its relevance for passive cooling applications (Section 2.3.3).

2.3.1. Algorithm for effective reflectance calculation

The effective reflectance of a material can be indirectly estimated by integrating its optical and photometric properties, following the approach proposed by Chiatti et al. [37]. The correction method considers the reflectance spectra corresponding to the inactive and discharging states, and accounts for the discrepancy introduced by PL by isolating and correcting the PL-related contribution with respect to the inactive condition. The procedure begins with the identification of the radiance peak ($L_{e,max}$) and its corresponding wavelength (λ_{max}) using spectroradiometric measurements. Subsequently, solar spectrophotometric analyses are performed to determine the spectral reflectance at λ_{max} for both the inactive and discharging states. The difference between these reflectance values ($\Delta\rho(\lambda_{max})$) (Eq. (1)) is attributed to PL emission. This is due to the synchronization between the instrument's detection wavelength and the material's emission wavelength, and is thus correlated with the measured radiance peak $L_{e,max}$.

$$\Delta\rho(\lambda_{max}) = \rho_{disc}(\lambda_{max}) - \rho_{inact}(\lambda_{max}) \tag{1}$$

For all other wavelengths where PL occurs, a correction term is calculated as defined in Eq. (2) and added to reflectance value measured in inactive condition at the same wavelength.

$$\rho_{correct}(\lambda) = L_e(\lambda)\frac{\Delta\rho_{max}(\lambda_{max})}{L_{e,max}} \tag{2}$$

2.3.2. Validation of the analytical approach

A statistical validation was performed to assess the accuracy of the analytical correction in reproducing the experimental data. Specifically, the solar reflectance profiles obtained before and after applying the correction algorithm were compared with the effective reflectance measured under polychromatic excitation. Two widely adopted statistical indicators were used: (i) the root mean square error (RMSE), which provides a quantitative measure of the average prediction error (Eq. (3)), and (ii) the coefficient of determination (R^2), which assesses the overall goodness-of-fit.

$$RMSE = \sqrt{\frac{1}{n}\sum_{i=1}^{n}(\rho_{charging,i} - \rho_{correct,i})^2} \tag{3}$$

2.3.3. Cooling potential calculation

Energy flux calculations were performed for each sample in its charged and discharged states. The model proposed by Garshasbi et al. [51] was employed to compare the cooling potentials associated with varying PL content and emissions. In particular, the amount of solar irradiation absorbed by the sample in each state was calculated as a function of its effective absorptance (α^*) as follows:

$$\Phi_{inact} = \int_{300\ nm}^{2500\ nm} I(\lambda)\cdot\alpha(\lambda)\,d\lambda \tag{4}$$

$$\Phi_{char} = \int_{300\ nm}^{2500\ nm} I(\lambda)\cdot\alpha^*(\lambda)\,d\lambda \tag{5}$$

Specifically, the solar irradiance was calculated using power values per unit area (I) in the visible range from the ASTM G173-03 standard [52], which represents global solar irradiance on a 37° tilted surface. Both the absorptance(α) and effective absorptance of the samples were derived from their previously measured reflectance spectra as: $\alpha = 1-\rho-\tau; \alpha^* = 1-\rho^*-\tau^*$ (τ and τ^* are assumed equal to 0).

Cooling performance due to the PL phenomena was quantified as the difference between the absorbed energy flux in the inactive state (Φ_{disc}) and that in the charging (Φ_{act}) or discharging state (Φ_{char}), i.e., considering both PL and persistent PL contributions.

3. Experimental results

This section presents the experimental results obtained from the characterization of the investigated samples. First, profilometric measurements were conducted to assess the surface roughness and texture, which can influence both optical and thermal responses (Section 3.1). Section 3.2 discusses the results of spectrophotometric and spectroradiometric analyses, providing insights into the optical and emission properties of the samples under different PL conditions. Finally, thermal characterization completes the assessment by examining the infrared emissive behavior of the materials, offering a comprehensive evaluation of their potential as passive cooling surfaces (Section 3.3).

3.1. Surface morphology

Fig. 4 compares the samples' surfaces obtained by profilometric analysis, highlighting how an increasing amount of PL pigments significantly altered the superficial morphology of the samples. The effect of concentration on roughness was experimental assessed using the parameters suggested by ISO25178 standard (Table 2), consistent to [53]. The height parameters exhibit a clear trend of increasing surface roughness with higher pigment content. The root mean square height (Sq) and the maximum peak-to-valley height (Sz) rise substantially, indicating a more uneven surface. Meanwhile, kurtosis (Sku) decreases as the pigment concentration increases, suggesting a transition from sharp peaks and valleys to a more uniform height distribution.

The hybrid parameters further highlight the growing surface complexity with increased pigment content. The root mean square gradient (Sdq) rises from 0.10 at Y-7% to 3.22 at Y-70%, indicating steeper surface slopes. The increase in developed interfacial area ratio (Sdr) underscores the formation of a highly complex surface with significantly greater interfacial area. Conversely, the spatial parameters, providing additional insight into the surface texture, highlight no clear trend. As concentration increases, the pigment distribution remains homogeneous, providing isotropic surface with stable texture aspect ratio (Str).

3.2. Optical characterization

Solar reflectance profiles of the investigated samples were collected under three different conditions. Inactive samples (Fig. 5a) exhibited similar spectral profiles, with good reflectance performance up to 500 nm. A linear dependence on the content of photoluminescent pigments is observed, particularly in the near-infrared (NIR) region.

As previously mentioned, the obtained spectrophotometric data can be considered reliable for the inactive state of the material, but not during PL emission. Since the spectrophotometer employs monochromatic light as the excitation source, it assumes that the detected radiation

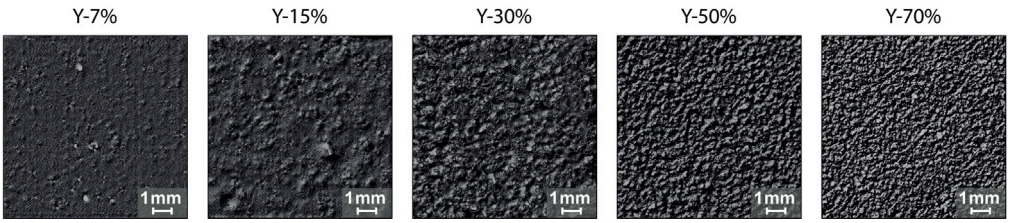

Fig. 4. Samples' surfaces analyzed by profilometric analysis.

Table 2
Results from the profilometric analysis.

Sample	Height parameters			Spatial parameters			Hybrid parameters	
	Sq [μm]	Sku [–]	Sz [μm]	Sal [μm]	Str [–]	Std [°]	Sdq [–]	Sdr [%]
Y-7%	0.90	20.42	12.66	106.52	0.86	16.75	0.10	0.49
Y-15%	1.92	18.69	36.46	231.98	0.92	93.25	0.18	1.35
Y-30%	16.63	16.52	324.58	249.77	0.89	86.75	1.38	40.66
Y-50%	41.15	6.00	527.45	174.64	0.92	0.01	2.18	90.48
Y-70%	73.52	5.65	870.49	152.15	0.94	8.50	3.22	162.11

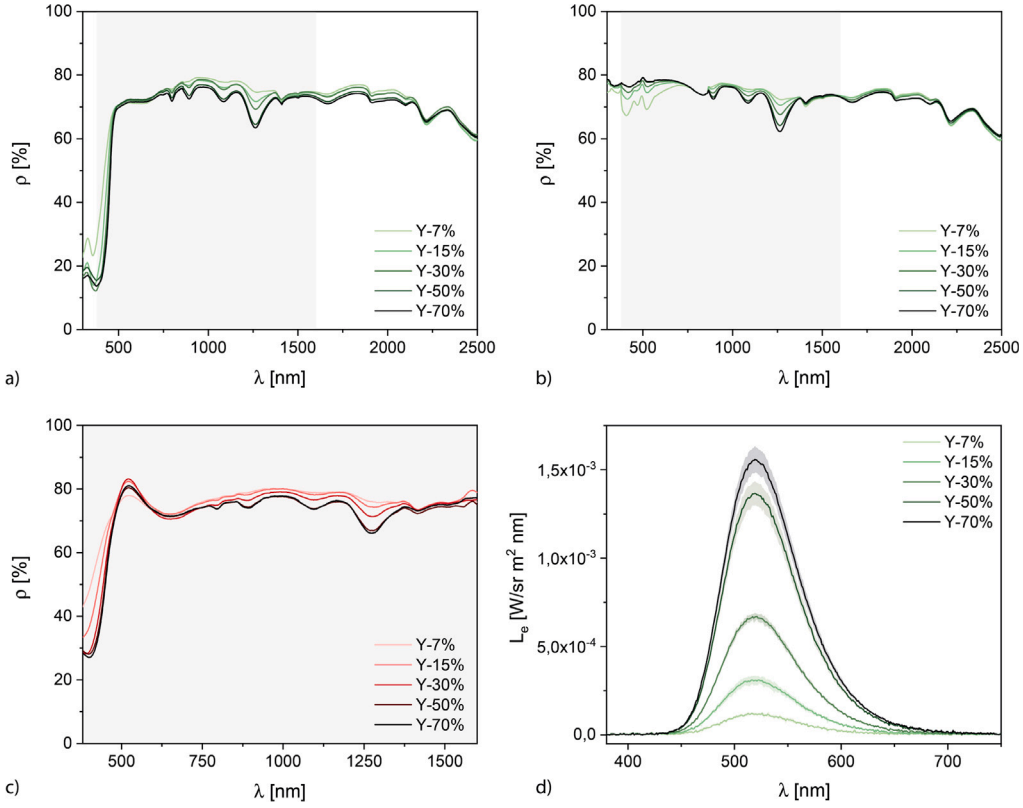

Fig. 5. Reflectance profiles of all investigated samples in their (a) inactive state, (b) discharging state soon after the end of exposure, (c) charging state under polychromatic excitation. (d) Spectral radiance profiles of investigated tiles soon after the end of the solicitation.

is only due to reflection of the incident light at the same wavelength. However, PL materials emit visible radiation at different wavelengths upon excitation, which can trigger the photodetector (e.g., photomultiplier tube), thereby introducing instrumental errors. Indeed, reflectance measurements taken in the discharging state, i.e., immediately after exposure in the climatic chamber, confirmed this issue. While reflectance values in the 860–2500 nm range remained comparable to the inactive state, a significant increase was detected in the UV and visible regions due to ongoing re-emission (Fig. 5b).

To address these limitations, a potential strategy involves the use of spectrophotometers equipped with polychromatic light sources. Fig. 5c displays the reflectance values of the investigated samples in their charging state. A pronounced peak around 520 nm is observed across all samples, corresponding to the PL emission. Notably, the enhancement in reflectance within this emission band does not scale linearly with pigment concentration: the Y-15% and Y-30% samples outperform the more heavily pigmented tiles. Also in this case, reflectance profiles in the NIR wavelengths remained similar to the inactive state.

Fig. 5d compares the spectral radiance profiles of all investigated samples shortly after the end of the exposure in the climatic chamber. The afterglow intensity (L_e and L_v) increased with the percentage of pigment, with emission peaks consistently centered between 519 and 521 nm across all samples. The PL decay times were determined following the procedure outlined in the DIN 67510-1 standard. By plotting

Table 3
PL emission and decay characterization.

Sample	L_e [W/sr m^2]	λ_{peak} [nm]	$L_{v,t=0}$ [cd/m^2]	Time to 0.03 cd/m^2	Data fitting curve y = log(L_v); x = log(t)	R^2
Y-7%	0.01	519	5.8	6.25 min	$y = 0.027x^2-0.992x+0.854$	0.980
Y-15%	0.03	521	15.1	19.04 min	$y = -0.048x^2-0.757x+1.240$	0.991
Y-30%	0.06	521	32.5	28.82 min	$y = -0.092x^2-0.662x+1.581$	0.991
Y-50%	0.12	521	66.5	41.86 min	$y = -0.068x^2-0.773x+1.889$	0.997
Y-70%	0.14	520	75.7	32.95 min	$y = -0.103x^2-0.713x+1.947$	0.997

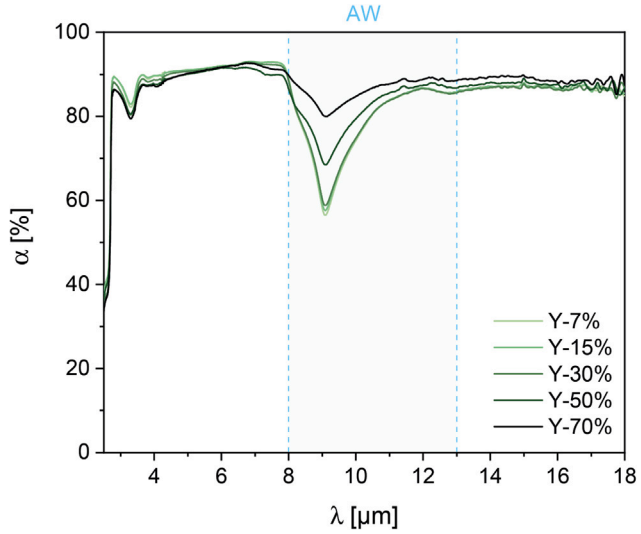

Fig. 6. Absorptance profiles in the MIR wavelengths.

the logarithmic luminance values over time, a second-order polynomial curve was fitted to the experimental data. The photoluminescence decay time, corresponding to a luminance of 0.03 cd/m^2, was then derived from the fitted curve, as reported in Table 3. Results showed that higher initial luminance, resulting from increased pigment concentrations, did not necessarily correlate with longer afterglow durations. Indeed, the Y-50% sample exhibited the longest photoluminescence decay time (41 min and 52 s).

3.3. Thermal characterization

All samples exhibited excellent broadband thermal emissivity ($\epsilon \geq 0.90$), with a slight increase observed at higher pigment concentrations, as shown in Fig. 6. Although the differences in total emissivity remain relatively small, the spectral variations due to the Al–O vibrational modes within the PL host matrix (9.12 μm) [54] are much more pronounced, exceeding 20% as the pigment concentration increases. This emissivity enhancement is expected to contribute favorably to the cooling performance, since this absorption band falls within the atmospheric window (8–13 μm), and therefore increases the net radiative heat flux towards the outer space. Consequently, optimizing pigment content not only influences the optical and PL properties, but could also play a role in tailoring thermal emission for passive daytime radiative cooling applications.

4. Critical analysis of the results

This section presents a critical discussion of the results obtained through the implementation of the correction methodology and its implications for evaluating PL materials. Specifically, Section 4.1 focuses on the application of the correction algorithm and its validation through the comparison with experimental data. Once the changes in the ESR have been reliably assessed, it becomes possible to quantify the impact on PL on the surface energy balance. This evaluation represents a crucial step towards the practical implementation of PL materials in urban environments, where their ability to reduce heat accumulation can contribute significantly to mitigating the UHI effect (Section 4.2).

4.1. Evaluation of correction performance

The correction procedure described in 2.3.1, designed to analytically determine the effective reflectance of investigated PL samples during the afterglow evolution, was applied to the experimental data. The PL effect induces peaks around 520 nm across all samples, corresponding to the PL emission. Fig. 7 compares the calculated ρ^* profiles for each tile, highlighting a direct dependence with the percentage of pigments in the samples.

The corresponding thermal effect due to the ongoing thermal emission could be quantified by calculating the surface temperature of a hypothetical building roof made of the investigated material, moving from the solar reflectance index (SRI) determined following the standard ASTM E1980 [49]. Since the conventional SRI formulation does not explicitly account for selective optical phenomena [55], such as PL, the notation SRI_{PL} is used to indicate values obtained for materials exhibiting PL re-emission. Therefore, coupling (i) the previously determined thermal emissivity and (ii) the solar reflectance value of both the inactive and discharged state, SRI and SRI_{PL} values were determined for each tile (Table 4). A temperature difference of approximately −0.4°C to −0.6°C is observed between the surface in the discharging state, i.e., with PL in progress, and its inactive counterpart.

To assess the effectiveness of the proposed correction, a baseline comparison was introduced by directly evaluating the agreement between the non-corrected monochromatic spectra and the corresponding polychromatic (charging) spectra. As reported in Table 5, this uncorrected comparison yields relatively high RMSE values (up to 11.6%) and very low coefficients of determination ($R^2 \leq 0.38$), indicating poor agreement. In contrast, after applying the proposed correction, the RMSE is consistently reduced to values below 4%, while R^2 increases to values above 0.96 for all samples. These results demonstrate that the proposed method provides for a substantial and systematic improvement over the uncorrected estimator, validating its ability to accurately reconstruct the polychromatic response.

Fig. 8 compares the ρ^* profiles of all investigated samples (i) as obtained through the correction algorithm, and (ii) the charging state, experimentally measured under direct polychromatic exposure. In the NIR region, the profiles exhibit minimal differences, remaining within the instrumental error. In the visible range, the peaks associated with PL emissions show excellent agreement for samples with higher pigment concentrations. Conversely, larger discrepancies are observed in the less concentrated samples, particularly for Y-15%. These variations arise from the different states under which the samples are characterized: charging samples are tested under direct irradiation, whereas discharging samples are measured during the afterglow phase. In this context, the shorter afterglow duration and lower emission intensity of less concentrated samples have a more pronounced effect compared to those with higher pigment concentrations. Therefore, the transition time between the charging setup and the spectrophotometer, as well as the measurement speed, should be considered relative to the PL decay time. While for persistent phosphors with lifetimes on the order of

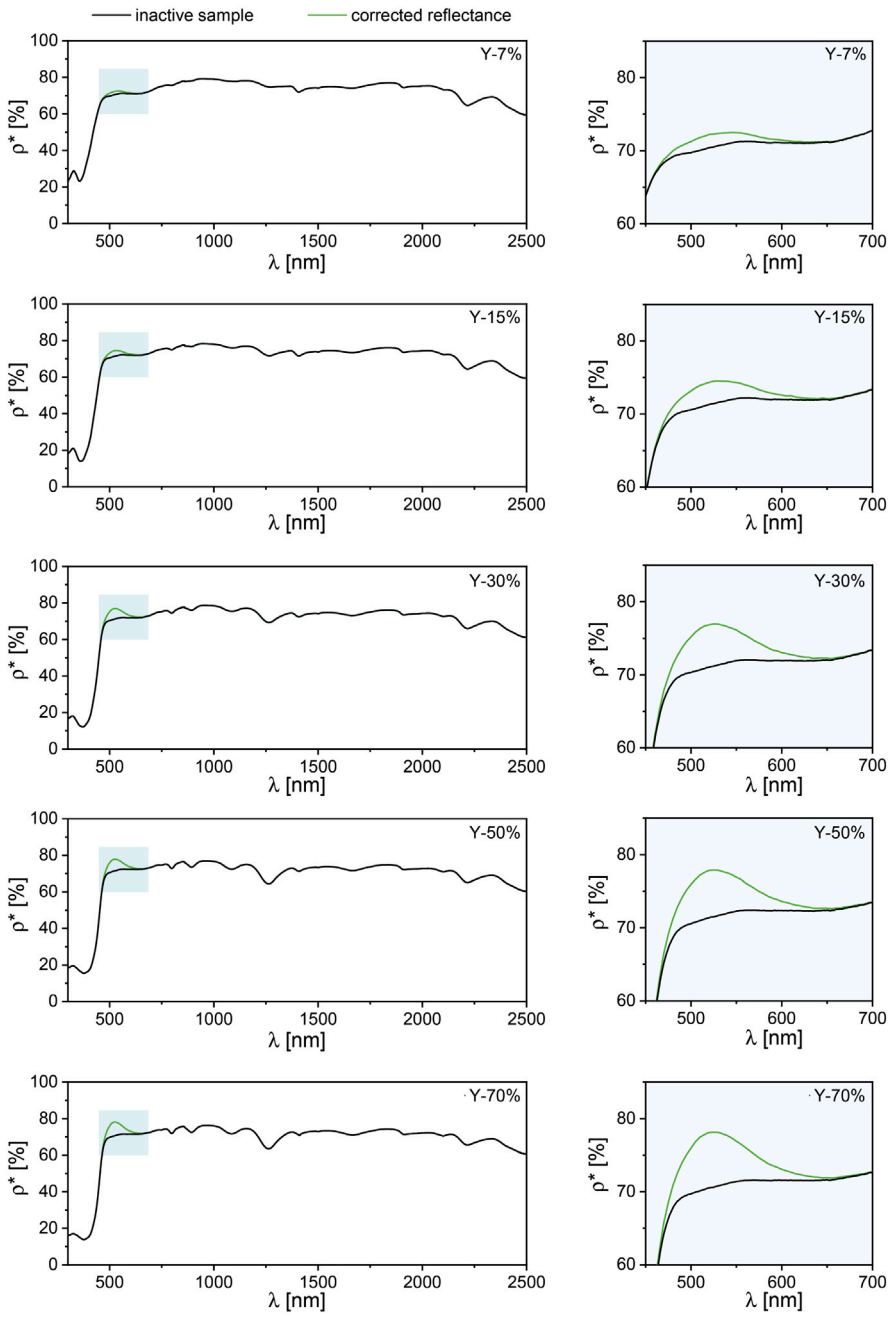

Fig. 7. Comparison between the effective reflectance measured in the inactive state and the reflectance immediately after excitation, computed through the correction algorithm.

Table 4
Determination of SRI values and corresponding superficial temperatures in inactive and discharging states for each sample.

Sample	Inactive					Discharging				
	ρ_{sol}	ρ_{vis}	ϵ	SRI [h_c = 12]	T_{sup} [°C]	ρ^*_{sol}	ρ^*_{vis}	ϵ	SRI_{PL} [h_c = 12]	T_{sup} [°C]
Y-7%	0.70	0.71	0.90	86	50.0	0.71	0.72	0.90	87	49.4
Y-15%	0.69	0.72	0.90	84	50.5	0.70	0.73	0.90	86	50.0
Y-30%	0.68	0.71	0.91	83	50.9	0.69	0.75	0.91	85	50.4
Y-50%	0.67	0.72	0.91	82	51.4	0.68	0.75	0.91	83	50.9
Y-70%	0.66	0.71	0.91	81	52.0	0.67	0.75	0.91	82	51.4

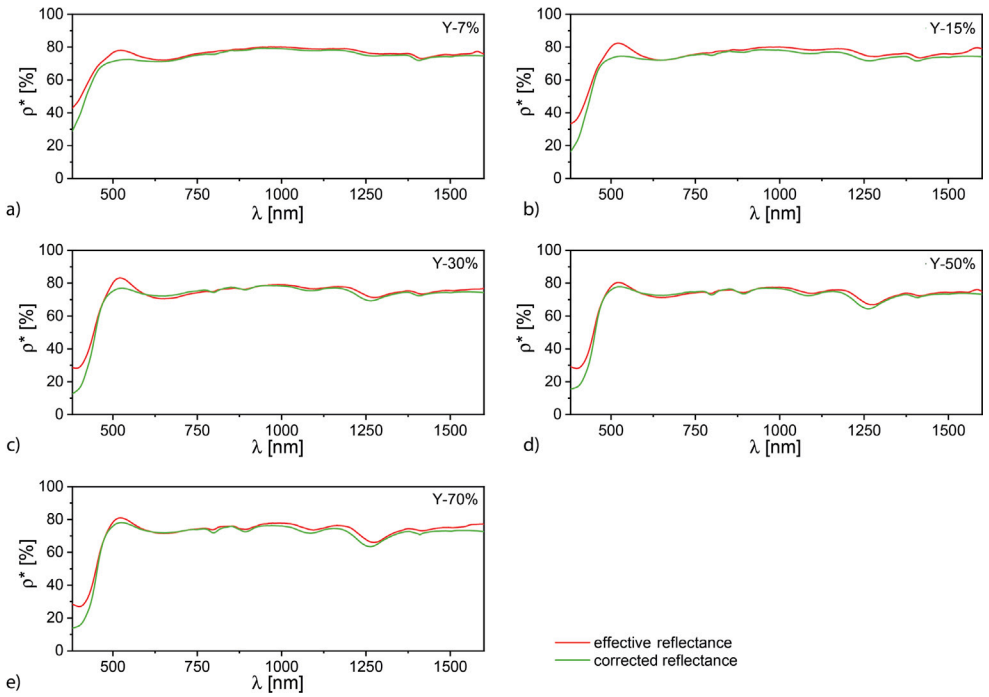

Fig. 8. Comparison between the ρ^* profiles obtained through the correction algorithm and experimentally collected during charging state under polychromatic excitation.

Table 5
Validation metrics between experimental and analytical solar reflectance curves for the investigated samples.

Sample	Non corrected/polychromatic		Corrected/polychromatic	
	RMSE (%)	R^2	RMSE (%)	R^2
Y-7%	5.2	0.38	2.8	0.98
Y-15%	8.3	0.04	3.8	0.96
Y-30%	10.6	0.01	3.2	0.97
Y-50%	11.2	0.01	2.8	0.99
Y-70%	11.6	0.01	3.2	0.99

minutes this introduces only minor uncertainty, for materials with significantly shorter decay times the timing of the measurement becomes a critical factor.

This behavior is also evident during the discharging phase of the sample, as it undergoes persistent luminescence decay, as shown in Fig. 9 for sample Y-70%. The sample's ability to reject solar radiation through both reflection and PL(ρ^*) reached its maximum under direct irradiation and gradually declined in accordance with the PL decay, as determined by spectroradiometric analysis.

An increase in reflectance in the UV range was observed when measuring the samples under polychromatic excitation, compared to the discharging state where only PL decay occurs. This behavior can be attributed to the long relaxation times of the PL pigments. Under simultaneous irradiation, in fact, a fraction of the pigments remains in the excited state, temporarily unavailable to absorb additional light. The polychromatic measurement thus provides for a more realistic representation of the actual PL contribution, particularly under outdoor conditions with direct sunlight, highlighting the limitations of conventional spectrophotometers employing monochromatic excitation.

4.2. Quantification of PL cooling potential

Assessing the changes in the effective reflectance ρ^*, and thus their effects on the energy balance of a surface, is a crucial step towards the implementation of PL materials for UHI mitigation. For this reason, the procedure presented in Section 2.3.2 was performed to quantify the cooling potential exploited by the samples in different PL states. Fig. 10 compares the solar radiation absorbed by each tile in its inactive (Φ_{inact}), charging (PL, Φ_{char}) and discharging state, immediately after the end of the solicitation (persistent PL, Φ_{disc}). The difference in area between the inactive and charging/discharging curves indicates the radiative flux (W/m^2) emitted by the PL samples in each state (Table 6). Notably, the cooling power due to PL emission is consistently higher for all samples under direct solar excitation, when PL occurs simultaneously with excitation. This condition represents the most relevant scenario for UHI mitigation, as it maximizes re-emission during daytime, i.e., when solar irradiation leads to the undesired surface overheating.

As previously observed during the algorithm application, the radiative performance under persistent PL conditions appears to be linearly related to the concentration of PL pigments in the tiles, increasing from 2.55 W/m^2 for the Y-7% tile up to the 10.62 W/m^2 for the Y-70% sample. Conversely, under direct polychromatic irradiation, no clear linear trend was observed, with smaller variations across the samples due to the influence of PL emission. Under these conditions, the best performance was achieved by the Y-15% sample in terms of both ρ^* (0.78) and PL radiative flux (23.34 W/m^2). This result confirmed the hypothesis proposed by Chiatti et al. [37] regarding the existence of an optimal concentration level for PL pigments in real-scale prototype materials, such as these tested tiles. While a higher pigment concentration enhances phosphorescence performance in terms of luminous intensity and afterglow duration, it also affects the surface roughness and the scattering strength of the coating. As a consequence, the probability of self-absorption mechanisms increases, leading to a quenching of the PL emission. Therefore, the optimization of PL pigments concentration needs to be deeply investigated to guarantee the best performance, balancing net cooling power and afterglow intensity. Moreover, a rougher surface is more prone to dusting and soiling, potentially resulting in reduced solar reflectance with time and lower PL emission due to decreased excitation of the luminescent material. This effect may also imply higher maintenance requirements over the service life of the coating.

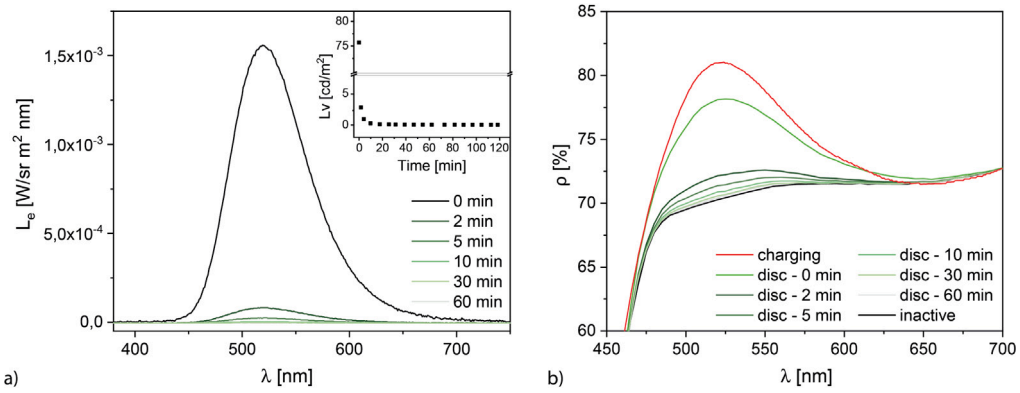

Fig. 9. (a) Afterglow decay of Y-70% sample, (b) Effective reflectance decay of the Y-70% tile through time from the end of the solicitation.

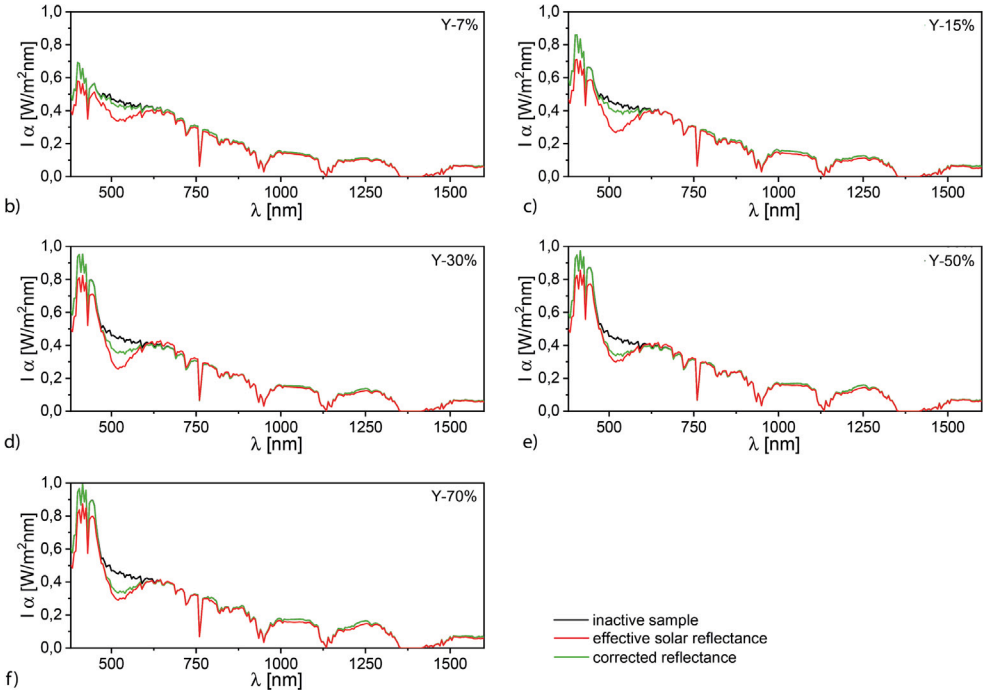

Fig. 10. Comparison between the solar radiation absorbed by each tile in its inactive, charging (photoluminescence) and discharging state, immediately after the end of the solicitation (persistent photoluminescence).

Table 6
Cooling potential of investigated samples according to different PL conditions.

Sample	Inactive		Photoluminescence			Persistent PL		
	ρ_{vis}	Φ_{inact} [W/m^2]	ρ^*_{vis}	Φ_{char} [W/m^2]	$\Delta\Phi_{inact-char}$ [W/m^2]	ρ^*_{vis}	Φ_{disc} [W/m^2]	$\Delta\Phi_{inact-disc}$ [W/m^2]
Y-7%	0.71	164.03	0.75	144.81	19.22	0.72	161.48	2.55
Y-15%	0.72	170.90	0.78	147.56	23.34	0.73	166.55	4.35
Y-30%	0.71	179.20	0.77	159.50	19.71	0.75	171.06	8.15
Y-50%	0.72	181.17	0.76	164.01	17.16	0.75	172.15	9.02
Y-70%	0.71	186.10	0.76	164.71	21.38	0.75	175.47	10.62

Table 7
Comparison of cooling potential offered by different passive cooling strategies.

Ref.	Cooling strategy	Material	Cooling potential [W/m^2]
This work	PL	$SrAl_2O_4$: Eu^{2+},Dy^{3+}	19–23
[37]	PL	$SrAl_2O_4$: Eu^{2+},Dy^{3+}	5–27
[19]	PL	CIS/ZnS QDs	35–54
[35]	PL	$Sr_2Si_5N_8$: Eu^{2+}, $Y_3Al_5O_{12}$: Ce^{3+}, (Ba,Sr)SiO_4 : Eu^{2+} + SiO_2 in PSA	38–46
[56]	RC - PL	Al substrate + TiO_2 - $SrAl_2O_4$: Eu^{2+},Dy^{3+}, Yb^{3+} in PSA	84
[21]	RC - PL	CA/$CsPbX_3$ (X = Br,I)	26–52
[57]	RC - PL	$CuGaS_2$/ZnS QDs, $CuInS_2$/ZnS QDs, $CuInSe_2$/ZnS QD Cu-based QDs in H–SiO_2/PVDF-HFP, PMMA	14–44
[18]	RC - PL	Ag substrate - CdSe/ZnS core–shell NCs in PDMS	62
[58]	RC	Al substrate - anodic aluminum oxide	64
[59]	RC	$BaSO_4$ acrylic paint	117

As summarized in Table 7, the cooling potential achieved in this work (19–23 W/m^2) is consistent with previously reported values for PL coatings. More recent phosphor systems embedded in polymer matrices also fall within a similar range (38–46 W/m^2) [35]. These results confirm that PL conversion can provide a non-negligible extra cooling contribution through the wavelength conversion mechanism, even in colored or semi-transparent systems where solar reflectance is intrinsically limited, and that may disclose much larger applicability potential due to aesthetic reason.

Furthermore, PL conversion can be synergistically combined with reflective or thermally emissive layers within composite devices, offering promising pathways towards tunable and multifunctional radiative cooling materials. Reported values range up to approximately 84 W/m^2, depending on the specific design strategy, PL system, and substrate properties, which are comparable to those achieved by radiative coolers based on ultra-white coatings.

5. Conclusions

In the last years, PL materials have become a valid strategy for passive cooling of the built environment due their ability to re-emit photons instead of phonons, and thus reducing surface temperatures under solar exposure. However, experimentally quantifying the PL contribution on a surface's energy balance is still difficult, limiting their reliable and replicable application in urban environments. For the first time, this study experimentally validated an innovative procedure based on optical and photometric measurements to determine the effective solar reflectance of ceramic tiles with different concentrations of yellow-emitting pigments.

The main findings of this study can be summarized as follows:

- The accuracy of the analytical correction in reproducing experimental reflectance data was confirmed through statistical validation (RMSE $\leq$ 3% and $R^2 \geq 0.96$).
- Higher PL pigment content boosts afterglow but may reduce net cooling under sunlight due to increasing surface roughness and the scattering strength of the coating.
- Under direct polychromatic irradiation, the best performance was achieved by the Y-15% sample in terms of both ρ^* (0.78) and PL radiative flux (23.34 W/m^2).
- By enabling manufacturers and researchers to reliably quantify PL-assisted reflectance, this experimentally validated methodology may support the development of future test guidelines and certification schemes for cool materials exploiting photoluminescent re-emission.

CRediT authorship contribution statement

Francesco Marchini: Writing – original draft, Visualization, Validation, Software, Investigation, Formal analysis, Data curation. **Chiara Chiatti:** Writing – review & editing, Validation, Investigation. **Claudia Fabiani:** Writing – review & editing, Validation, Supervision, Methodology, Investigation, Conceptualization. **Michele Zinzi:** Writing – review & editing, Supervision, Resources, Investigation, Formal analysis, Data curation. **Anna Laura Pisello:** Writing – review & editing, Supervision, Resources, Project administration, Investigation, Funding acquisition.

Declaration of competing interest

The authors declare that they have no known competing financial interests or personal relationships that could have appeared to influence the work reported in this paper.

Acknowledgments

This research has received funding from the European Research Council (ERC) under the European Union's Horizon Europe research and innovation programme (ERC-2021-STG, HELIOS, G.A. 101041255 and ERC-2024-POC FOR REAL G.A. 101213070). Views and opinions expressed are however those of the authors only and do not necessarily reflect those of the European Union or the European Research Council. Neither the European Union nor the granting authority can be held responsible for them. This research has received funding from Project 1.5 "High-efficiency buildings for the energy transition" within the "Electrical System Research" Programme Agreements 25-27 between ENEA and the Ministry of Environment (PTR 25-27). F.M.'s acknowledgments are due to the National Ph.D. course in Photoinduced Processes and Technologies from the University of Perugia.

Data availability

Data will be made available on request.

References

[1] International Energy Agency, Empowering Cities for a Net Zero Future: Unlocking Resilient, Smart, Sustainable Urban Energy Systems, OECD Publishing, 2021.
[2] M. Moore, P. Gould, B.S. Keary, Global urbanization and impact on health, Int. J. Hyg. Env. Health 206 (4–5) (2003) 269–278, http://dx.doi.org/10.1078/1438-4639-00223.
[3] S. Chapman, J.E. Watson, A. Salazar, M. Thatcher, C.A. McAlpine, The impact of urbanization and climate change on urban temperatures: a systematic review, Landsc. Ecol. 32 (2017) 1921–1935, http://dx.doi.org/10.1007/s10980-017-0561-4.
[4] Z. Ouyang, P. Sciusco, T. Jiao, S. Feron, C. Lei, F. Li, R. John, P. Fan, X. Li, C. Williams, G. Chen, C. Wang, J. Chen, Albedo changes caused by future urbanization contribute to global warming, Nat. Commun. 13 (2022) 1234567890, http://dx.doi.org/10.1038/s41467-022-31558-z.
[5] C. Yuan, A.S. Adelia, S. Mei, W. He, X.-X. Li, L. Norford, Mitigating intensity of urban heat island by better understanding on urban morphology and anthropogenic heat dispersion, Build. Env. 176 (2020) 106876, http://dx.doi.org/10.1016/j.buildenv.2020.106876.

[6] D.S. Nasir, C.A.J. Pantua, B. Zhou, B. Vital, J. Calautit, B. Hughes, Numerical analysis of an urban road pavement solar collector (u-RPSC) for heat island mitigation: Impact on the urban environment, Renew. Energy 164 (2021) 618–641, http://dx.doi.org/10.1016/j.renene.2020.07.107.

[7] N. Yadav, K. Rajendra, A. Awasthi, C. Singh, B. Bhushan, Systematic exploration of heat wave impact on mortality and urban heat island: A review from 2000 to 2022, Urban Clim. 51 (2023) 101622, http://dx.doi.org/10.1016/j.uclim.2023.101622.

[8] M. Zinzi, E. Carnielo, B. Mattoni, On the relation between urban climate and energy performance of buildings. A three-years experience in Rome, Italy, Appl. Energy 221 (2018) 148–160, http://dx.doi.org/10.1016/j.apenergy.2018.03.192.

[9] M. Santamouris, G.Y. Yun, Recent development and research priorities on cool and super cool materials to mitigate urban heat island, Renew. Energy 161 (2020) 792–807, http://dx.doi.org/10.1016/j.renene.2020.07.109.

[10] M. Santamouris, A. Synnefa, T. Karlessi, Using advanced cool materials in the urban built environment to mitigate heat islands and improve thermal comfort conditions, Sol. Energy 85 (12) (2011) 3085–3102, http://dx.doi.org/10.1016/j.solener.2010.12.023.

[11] K. Feng, Y. Wu, X. Pei, F. Zhou, Passive daytime radiative cooling: from mechanism to materials and applications, Mater. Today Energy 43 (2024) 101575, http://dx.doi.org/10.1016/j.mtener.2024.101575.

[12] K.L. Uemoto, N.M. Sato, V.M. John, Estimating thermal performance of cool colored paints, En. Build. 42 (1) (2010) 17–22, http://dx.doi.org/10.1016/j.enbuild.2009.07.026.

[13] N. Wang, Y. Lv, D. Zhao, W. Zhao, J. Xu, R. Yang, Performance evaluation of radiative cooling for commercial-scale warehouse, Mater. Today Energy 24 (2022) 100927, http://dx.doi.org/10.1016/j.mtener.2021.100927.

[14] I. Kousis, A.L. Pisello, Toward the scaling up of daytime radiative coolers: A review, Adv. Opt. Mater. 11 (21) (2023) 2300123, http://dx.doi.org/10.1002/adom.202300123.

[15] A. Khan, L. Carlosena, S. Khorat, R. Khatun, Q.-V. Doan, J. Feng, M. Santamouris, On the winter overcooling penalty of super cool photonic materials in cities, Sol. Energy Adv. 1 (2021) 100009, http://dx.doi.org/10.1016/j.seja.2021.100009.

[16] K. Lin, J. Chen, A. Pan, H. Li, Y. Fu, C.T. Kwok, L. Liang, L. Chao, Y. Zhu, Q. Sun, C.Y. Tso, Beyond the static: dynamic radiative cooling materials and applications, Mater. Today Energy 44 (2024) 101647, http://dx.doi.org/10.1016/j.mtener.2024.101647.

[17] M. Luo, J. Song, Z. Ling, Z. Zhang, X. Fang, Phase change material coat for battery thermal management with integrated rapid heating and cooling functions from −40 °C to 50 °C, Mater. Today Energy 20 (2021) 100652, http://dx.doi.org/10.1016/j.mtener.2021.100652.

[18] S. Son, S. Jeon, J. Bae, S. Lee, D. Chae, J.-Y. Chae, T. Paik, H. Lee, S. Oh, Efficient radiative cooling emitter adopting the wavelength conversion of giant CdSe/ZnS core-shell nanocrystals, Mater. Today Phys. 21 (2021) 100496, http://dx.doi.org/10.1016/j.mtphys.2021.100496.

[19] S. Garshasbi, S. Huang, J. Valenta, M. Santamouris, Can quantum dots help to mitigate urban overheating? An experimental and modelling study, Sol. Energy 206 (2020) 308–316, http://dx.doi.org/10.1016/j.solener.2020.06.010.

[20] F. Marchini, R. Bondi, A. Duri, C. Fabiani, L. Latterini, A.L. Pisello, Coupling vanadium oxide and lead-free perovskite for sustainable passive daytime radiative cooling, Renew. Energy 256 (2026) 123755, http://dx.doi.org/10.1016/j.renene.2025.123755.

[21] X. Wang, Q. Zhang, S. Wang, C. Jin, B. Zhu, Y. Su, X. Dong, J. Liang, Z. Lu, L. Zhou, W. Li, S. Zhu, J. Zhu, Sub-ambient full-color passive radiative cooling under sunlight based on efficient quantum-dot photoluminescence, Sci. Bull. (ISSN: 2095-9273) 67 (18) (2022) 1874–1881, http://dx.doi.org/10.1016/j.scib.2022.08.028.

[22] C. Chiatti, C. Fabiani, A.L. Pisello, Long persistent luminescence: A road map toward promising future developments in energy and environmental science, Annu. Rev. Mater. Res. 51 (Volume 51, 2021) (2021) 409–433, http://dx.doi.org/10.1146/annurev-matsci-091520-011838.

[23] P. Berdahl, S.S. Chen, H. Destaillats, T.W. Kirchstetter, R.M. Levinson, M.A. Zalich, Fluorescent cooling of objects exposed to sunlight – The ruby example, Sol. Energy Mater. Sol. Cells 157 (2016) 312–317, http://dx.doi.org/10.1016/j.solmat.2016.05.058.

[24] M. Santamouris, H.S. Khan, R. Paolini, O.M.L. Julia, S. Garshasbi, I. Papakonstantinou, J. Valenta, Recent advances in fluorescence-based colored passive daytime radiative cooling for heat mitigation, Int. J. Thermophys. 45 (2024) 90, http://dx.doi.org/10.1007/s10765-024-03382-8.

[25] S. Min, S. Jeon, K. Yun, J. Shin, All-color sub-ambient radiative cooling based on photoluminescence, ACS Photonics 9 (4) (2022) 1196–1205, http://dx.doi.org/10.1021/acsphotonics.1c01648.

[26] I. Kousis, C. Fabiani, L. Gobbi, A.L. Pisello, Phosphorescent-based pavements for counteracting urban overheating – A proof of concept, Sol. Energy 202 (2020) 540–552, http://dx.doi.org/10.1016/j.solener.2020.03.092.

[27] C. Chiatti, C. Fabiani, E. Bou-Zeid, A. Pisello, Evaluating the potential of persistent luminescence in counteracting urban overheating, J. Phys. Conf. Ser. 2685 (1) (2024) 012029, http://dx.doi.org/10.1088/1742-6596/2685/1/012029.

[28] C. Chiatti, F. Rosso, C. Fabiani, A.L. Pisello, Integrated energy performance of an innovative translucent photoluminescent building envelope for lighting energy storage, Sustain. Cities Soc. 75 (2021) 103234, http://dx.doi.org/10.1016/j.scs.2021.103234.

[29] F. Marchini, C. Chiatti, C. Fabiani, A. Pisello, Development of an innovative translucent–photoluminescent coating for smart windows applications: An experimental and numerical investigation, Renew. Sustain. Energy Rev. 184 (2023) 113530, http://dx.doi.org/10.1016/j.rser.2023.113530.

[30] C. Fabiani, C. Chiatti, A.L. Pisello, Development of photoluminescent composites for energy efficiency in smart outdoor lighting applications: An experimental and numerical investigation, Renew. Energy 172 (2021) 1–15, http://dx.doi.org/10.1016/j.renene.2021.02.071.

[31] A. Springsteen, Introduction to measurement of color of fluorescent materials, Anal. Chim. Acta 380 (2) (1999) 183–192, http://dx.doi.org/10.1016/S0003-2670(98)00578-9.

[32] J.C. Zwinkels, Metrology of photoluminescent materials, Metrologia 47 (2) (2010) S182, http://dx.doi.org/10.1088/0026-1394/47/2/S15.

[33] R. Levinson, S. Chen, C. Ferrari, P. Berdahl, J. Slack, Methods and instrumentation to measure the effective solar reflectance of fluorescent cool surfaces, En. Build. 152 (2017) 752–765, http://dx.doi.org/10.1016/j.enbuild.2016.11.007.

[34] D. Chae, S.Y. Lee, H. Lim, S. Son, J. Ha, J. Park, J.H. Park, S.J. Oh, H. Lee, Vivid colored cooling structure managing full solar spectrum via near-infrared reflection and photoluminescence, ACS Appl. Mater. Interfaces 15 (50) (2023) 58274–58285, http://dx.doi.org/10.1021/acsami.3c08790.

[35] X. Ma, Y. Fu, D. Liu, N. Yang, J.-G. Dai, D. Lei, Fluorescence-enabled colored bilayer subambient radiative cooling coatings, Adv. Opt. Mater. 12 (19) (2024) 2303296, http://dx.doi.org/10.1002/adom.202303296.

[36] J. Valenta, A. Fucikova, M. Greben, H.S. Khan, R. Paolini, S. Garshasbi, M. Santamouris, Radiometric characterization of daytime luminescent materials directly under the solar illumination, AIP Adv. 14 (10) (2024) 105113, http://dx.doi.org/10.1063/5.0235354.

[37] C. Chiatti, I. Kousis, C. Fabiani, A.L. Pisello, Effect of optimized photoluminescence on luminous and passive cooling potential: A new combined experimental and numerical approach applied to yellow-emitting glass tiles, Renew. Energy 196 (2022) 28–39, http://dx.doi.org/10.1016/j.renene.2022.06.027.

[38] R. Prosser, G. Arruda, Color Matching Spanning the Visible and Near-Infrared: Use of the Cubic Spline Function in Interpolation, United States Army Natick Research, Development and Engineering Center Natick, Massachusetts, 1989.

[39] C. Chiatti, C. Fabiani, X. Huang, E. Bou-Zeid, A.L. Pisello, Exploring the potential of phosphorescence for mitigating urban overheating: First time representation in an Urban Canopy Model, Appl. Energy 362 (2024) 122984, http://dx.doi.org/10.1016/j.apenergy.2024.122984.

[40] T. Matsuzawa, Y. Aoki, N. Takeuchi, Y. Murayama, A new long phosphorescent phosphor with high brightness, $SrAl_2O_4$:$Eu2^{2+}$,Dy^{3+}, J. Electrochem. Soc. 143 (8) (1996) 2670, http://dx.doi.org/10.1149/1.1837067.

[41] C. Fabiani, M. Gambucci, C. Chiatti, G. Zampini, L. Latterini, A.L. Pisello, Towards field implementation of photoluminescence in the built environment for passive cooling and lighting energy efficiency, Appl. Energy 324 (2022) 119687, http://dx.doi.org/10.1016/j.apenergy.2022.119687.

[42] Bright Materials srl, website link: https://brightmaterials.it/en/. (Access 06 January 2025).

[43] ISO 25178-2:2021, Geometrical Product Specifications (GPS)—Surface Texture: Areal—Part 2: Terms, Definitions and Surface Texture Parameters, International Organization for Standardization, Geneva, Switzerland, 2021.

[44] ASTM E903-12, Standard test method for solar absorptance, reflectance, and transmittance of materials using integrating spheres, 2012, http://dx.doi.org/10.1520/E0903-12.

[45] A. Maccari, M. Montecchi, F. Treppo, M. Zinzi, CATRAM: an apparatus for the optical characterization of advanced transparent materials, Appl. Opt. 37 (22) (1998) 5156–5161, http://dx.doi.org/10.1364/AO.37.005156.

[46] DIN 67510-1, Phosphorescent pigments and products-part 1: Measurement and marking at the producer, Dtsch. Inst. Norm. (2020).

[47] C. Chiatti, C. Fabiani, A.L. Pisello, Toward the energy optimization of smart lighting systems through the luminous potential of photoluminescence, Energy 266 (2023) 126346, http://dx.doi.org/10.1016/j.energy.2022.126346.

[48] ASTM C1371-21:, Standard test method for determination of emittance of materials near room temperature using portable emissometers, ASTM Int. (2021).

[49] ASTM E1980-19:, Standard practice for calculating solar reflectance index of horizontal and low-sloped opaque surfaces, 2019.

[50] ISO 9050:2003, Glass in Building — Determination of Light Transmittance, Solar Direct Transmittance, Total Solar Energy Transmittance, Ultraviolet Transmittance and Related Glazing Factors, International Organization for Standardization, Geneva, Switzerland, 2003.

[51] S. Garshasbi, S. Huang, J. Valenta, M. Santamouris, Enhancing the cooling potential of photoluminescent materials through evaluation of thermal and transmission loss mechanisms, Sci. Rep. 11 (2021) 14725, http://dx.doi.org/10.1038/s41598-021-94354-7.

[52] ASTM G173-03:2020, Standard tables for reference solar spectral irradiances, Am. Soc. Test. Mater. -ASTM Int. (2021).
[53] F. Marchini, C. Fabiani, L. Latterini, A.L. Pisello, Optimising surface morphology for enhanced radiative properties in thermal energy-efficient materials, Mater. Today Energy 45 (2024) 101660, http://dx.doi.org/10.1016/j.mtener.2024.101660.
[54] N.M. Thomas, E.I. Anila, Synthesis and characterisation of $SrAl_2O_4$: Eu^{3+} orange-red emitting nanoparticles, J. Fluoresc. 34 (2024) 1161–1169, http://dx.doi.org/10.1007/s10895-023-03351-8.
[55] C. Fabiani, A. Muscio, A.L. Pisello, Introducing the enhanced solar reflectance index (SRI*) for comprehensive evaluation of spectrally selective cool materials in real-world scenarios, Sustain. Energy Technol. Assess. 81 (2025) 104415, http://dx.doi.org/10.1016/j.seta.2025.104415.
[56] X. Xue, M. Qiu, Y. Li, Q.M. Zhang, S. Li, Z. Yang, C. Feng, W. Zhang, J.-G. Dai, D. Lei, W. Jin, L. Xu, T. Zhang, J. Qin, H. Wang, S. Fan, Creating an eco-friendly building coating with smart subambient radiative cooling, Adv. Mater. 32 (42) (2020) 1906751, http://dx.doi.org/10.1002/adma.201906751.
[57] T.Y. Yoon, S. Son, S. Min, D. Chae, H.Y. Woo, J.-Y. Chae, H. Lim, J. Shin, T. Paik, H. Lee, Colloidal deposition of colored daytime radiative cooling films using nanoparticle-based inks, Mater. Today Phys. 21 (2021) 100510, http://dx.doi.org/10.1016/j.mtphys.2021.100510.
[58] Y. Fu, J. Yang, Y. Su, W. Du, Y. Ma, Daytime passive radiative cooler using porous alumina, Sol. Energy Mater. Sol. Cells 191 (2019) 50–54, http://dx.doi.org/10.1016/j.solmat.2018.10.027.
[59] X. Li, J. Peoples, P. Yao, X. Ruan, Ultrawhite BaSO4 paints and films for remarkable daytime subambient radiative cooling, ACS Appl. Mater. Interfaces 13 (18) (2021) 21733–21739, http://dx.doi.org/10.1021/acsami.1c02368.